Available online at www.sciencedirect.com

jmr&t Journal of Materials Research and Technology

www.jmrt.com.br

Original Article

Influence of graphene content and nickel decoration on the microstructural and mechanical characteristics of the Cu/Sn–Ag–Cu/Cu soldered joint

R. Sayyadi[a], F. Khodabakhshi[b,*], N. Shahamat Javid[c], G. Khatibi[d]

[a] Department of Materials Science and Engineering, School of Engineering, Shiraz University, Zand Boulevard, Shiraz, Iran
[b] School of Metallurgy and Materials Engineering, College of Engineering, University of Tehran, P.O. Box 11155-4563, Tehran, Iran
[c] Faculty of Mathematics, Natural Sciences and Materials Engineering, University of Augsburg, Augsburg, Germany
[d] Christian Doppler Laboratory for Lifetime and Reliability of Interfaces in Complex Multi-Material Electronics, Institute of Chemical Technologies and Analytics, Vienna University of Technology, Getreidemarkt 9/164, A-1060 Vienna, Austria

ARTICLE INFO

Article history:
Received 2 March 2020
Accepted 8 June 2020
Available online 23 June 2020

Keywords:
Sn–Ag–Cu (SAC) alloy
Graphene nanoplatelets (GNPs)
Nanocomposite lead-free soldering
Ni-coating
Physical property
Mechanical behavior

ABSTRACT

In this research article, lead-free nanocomposite soldering is assessed by using the eutectic composition of Sn-3.5Ag-0.7Cu (SAC, wt%) solder alloy as the matrix and graphene nanoplatelets (GNPs) as the reinforcing agent. Powders of these materials are mixed in a mechanical milling system, then compacted, and sintered before application. The effects of GNPs content with different amounts of 0.05, 0.1, and 0.2 wt% are examined to prepare nanocomposite solders as compared to the SAC solder alloy. Furthermore, to improve the metallurgical compatibility between the graphene and SAC solder matrix, the surface of GNPs was decorated by nickel particles using electroless plating techniques before incorporation. After that, the solderability of these prepared lead-free nanocomposite solders is investigated on the copper substrate. As the main result, the formation of the intermetallic compound (IMC) layers at the interface between the Cu-substrate and solder material was found very determinative to control the mechanical performance of soldered joints during lap-shear testing. The content of GNPs and Ni-coating modification strongly affected the morphology and growth of IMC layers at the interface. By increasing the amount of GNPs up to ~0.2 wt% and using Ni-coating, the growth of IMC layers was considerably suppressed, leading to a significant improvement of the joint strength up to ~27%, despite a reduction of ~50% of the ductility. Furthermore, isothermal aging at 150 °C up to 100 h resulted in a remarkable increase in the shear strength (~45%) and elongation to failure (~19.9%) through controlling the growth of the IMC layers at the interface.

* *Corresponding author.*
E-mail: fkhodabakhshi@ut.ac.ir (F. Khodabakhshi).
https://doi.org/10.1016/j.jmrt.2020.06.026

1. Introduction

In the electronic industry, the production of thermally stable connections withstanding the thermal fatigue phenomenon during the service is a challenging task [1]. Commonly, the mechanical performance of electronic components is strongly affected by the strength of the solder joints, which are considered as one of the weakest parts of these systems [1]. Within the last decade, considering the environment compatibility issues, lead-free solders have been developed to terminate the application of solders containing the Pb element [2]. Since then, researches have been focused on the development of lead-free solders with improved physical and mechanical durability as suitable candidates for low-temperature bonding [1]. In this regard, considering the low melting point of tin and the possibility to control the wettability by the addition of some alloying elements, several Sn-based lead-free solder systems have been introduced [3,4]. Depending on the application type and the required specifications, alloying elements such as bismuth, silver, copper, zinc, indium, and nickel have been applied [5–11]. One of the exciting and famous solder systems in this field is a ternary eutectic alloy between tin, silver, and copper with a chemical composition or stoichiometry of 95.8Sn-3.5Ag-0.7Cu (in wt%) also called as SAC3507 [3,4,12,13]. The SAC3507 solder alloy provides a low melting temperature of ~220 °C with a proper wetting action. However, its application can be restricted by low strength and feeble fatigue resistance, especially at high temperatures during service conditions under cyclic heating of electronic connections [3,13].

One effective approach for enhancing the durability of SAC solder alloy is reinforcing the soft material matrix by uniform dispersion of solid secondary phase nanoparticles and fabrication of a nanocomposite [2]. Several reports were noted on using different reinforcing nano-sized agents for this kind of nanocomposite fabrication, such as; SiC [14–16], Al_2O_3 [17], TiC [18], Fe_2O_3 [19], TiO_2 [20,21], ZnO [22,23], Si_3N_4 [24,25], CeO_2 [26], Ag_3Sn [27], SnO_2 [28], ZrO_2 [29], La_2O_3 [30], $ZrSiO_4$ [31], and *etc.* By comparing the highlighted results in this regard in the literature, it can be found that the different reinforcing agents with different chemistry displayed different effectiveness on enhancing the thermal stability and mechanical strength of SAC solder alloy [2]. Commonly, the intermetallics displayed the best compatibility with the solder alloy matrix caused by the *in situ* mechanism of formation. On the other side, oxide-based solid nanoparticles are advantageous due to ease of attaining a uniform dispersion during the manufacturing. Meanwhile, carbide-based nanoparticles are also of interest because of their quite hard nature for processing solder matrix nanocomposites with superior mechanical properties. Recently, special attention was focused on using carbon-based structures as reinforcing agents, including carbon nanotubes and graphene, regarding the superior physical and mechanical properties of these materials [32,33]. Graphene as an exfoliated single layer of graphite (thickness <0.35 nm) is a new advanced 2D-material with a high aspect ratio, lightweight, and low cost, exhibiting a high thermal and electrical conductivity as well as extremely high strength of over than 130 GPa and Young's modulus of higher than 1000 GPa in the plane direction [34,35]. Graphene has an excellent potential to be used in photonic and electronic applications as well as employing as a reinforcing agent for the production of advanced nanocomposites [36]. Graphene has a wide application, such as; (i) enhanced performance of light-controlled conductive switching in hybrid cuprous oxide/reduced graphene oxide (Cu_2O/rGO) nanocomposites [37]; (ii) enhanced X-ray photon response in solution-synthesized $CsPbBr_3$ nanoparticles wrapped by reduced graphene oxide [38]; (iii) preparation of cubic Cu_2O nanoparticles wrapped by reduced graphene oxide for the efficient removal of rhodamine B [39]; (iv) tunable photoluminescence of water-soluble AgInZnS-graphene oxide (GO) nanocomposites and their application *in vivo* bio-imaging [40]. This interesting material can be synthesized in the experiment simply according to the Hummer's approach by exfoliation of graphene oxide (GO), chemically [41]. Graphene nanoplatelet (GNP) is defined as a combination of several free-standing graphene monolayers with a thickness higher than 10 nm and a larger diameter in the range of micron [33]. This new class of carbon-based material is an excellent candidate for incorporation as a reinforcing agent in the fabrication of metal-matrix nanocomposites [42–44].

Some limited reports on the literature were focused on the addition of graphene as the secondary phase reinforcing agent into the matrix of lead-free solder alloys for the production of nanocomposite solders [45–52]. In the primary researches by Xu et al. [48,50], graphene nanosheet was introduced as an active reinforcing agent for strengthening of Sn–Ag–Cu solder alloy matrix by controlling the interfacial chemical reactions and corrosion behavior at the interface with the copper substrate. Chen et al. [45] studied the microstructural details, and the mechanical properties of the graphene reinforced Sn–Ag–Cu solder alloy as a new solder nanocomposite. Next, in the works by Xu et al. [49,52] and Jing et al. [46], the surface of graphene nanosheets was modified by silver (Ag) coating before application as a reinforcing agent. In those researches, Ag nanoparticles were successfully decorated on the surface of nanosheets, and the influence of these Ag-modified graphene nanosheets on the formation and growth of intermetallic compound (IMC) layers through the Sn–Ag–Cu solder alloy matrix was investigated [46,49,52]. Also, the microstructural characteristics and mechanical performance of the soldered joints were studied with more details that showed some degree of improvement concerning the non-coated graphene [45,48,51]. Recently, some trial results were reported by Khodabakhshi et al. [51] and Wang et al. [47] on using nickel as a modification material on the surface to enhance the metallurgical compatibility between the graphene and SAC solder alloy matrix. However, more research studies would be required to reveal all aspects of the involved metallurgical phenomena, and also optimize the design and performance of modified nanocomposite solders.

Therefore, the main object of the current research is focusing on the development of this kind of new solder material as a system including Sn–Ag–Cu solder alloy reinforced with graphene nanoplatelets (GNPs) dealing by more details examination of soldering process parameters. The main novelties of this work as compared to previous reports can be emphasized into three different directions, as follow; (i) investigating the

Table 1 – Characteristics of the original materials.

Raw material	Company	Chemical purity	Average particle size	Morphology
Sn	Merck, Germany	99.9%	<63 μm	Particulate
Ag	Merck, Germany	99.99%	<20 μm	Particulate
Cu	Merck, Germany	99.5%	<20 μm	Particulate
Graphene	US Nano, USA	99.8%	<2 μm	Platelets

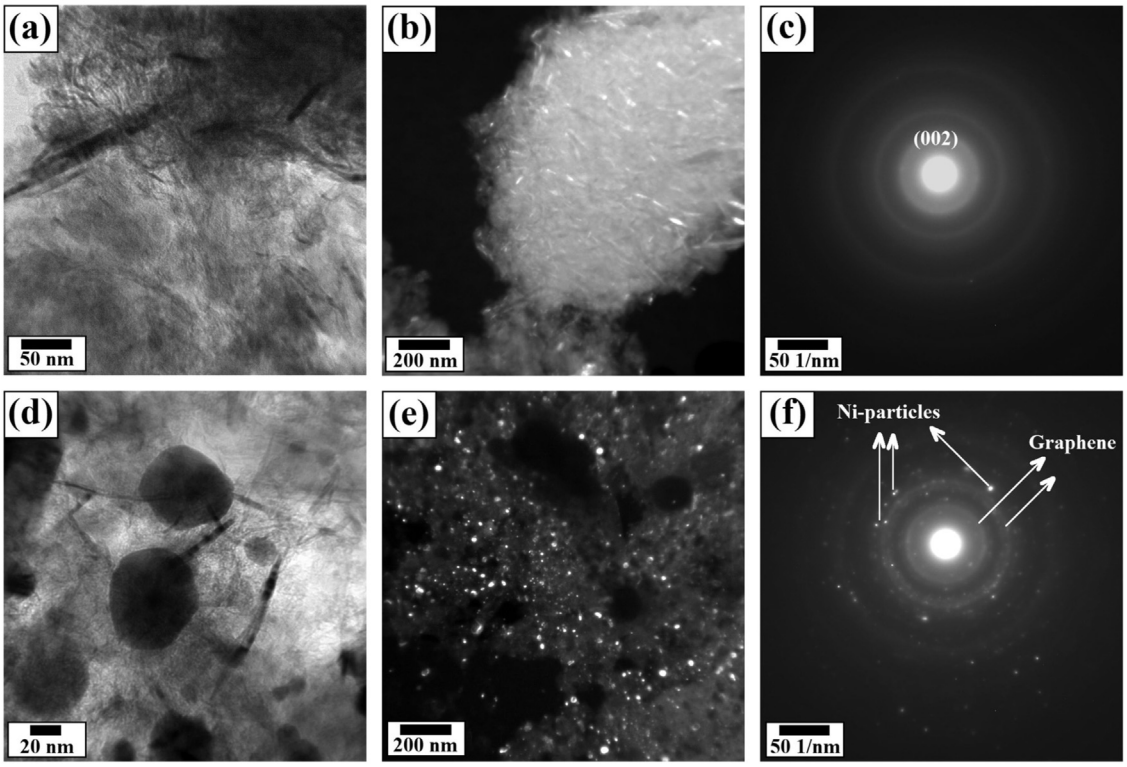

Fig. 1 – TEM results from GNPs (a–c) before and (d–f) after nickel electroless coating; (a, d) Bright-field TEMs images, (b, e) dark-field TEM images, and (c, f) SAD patterns.

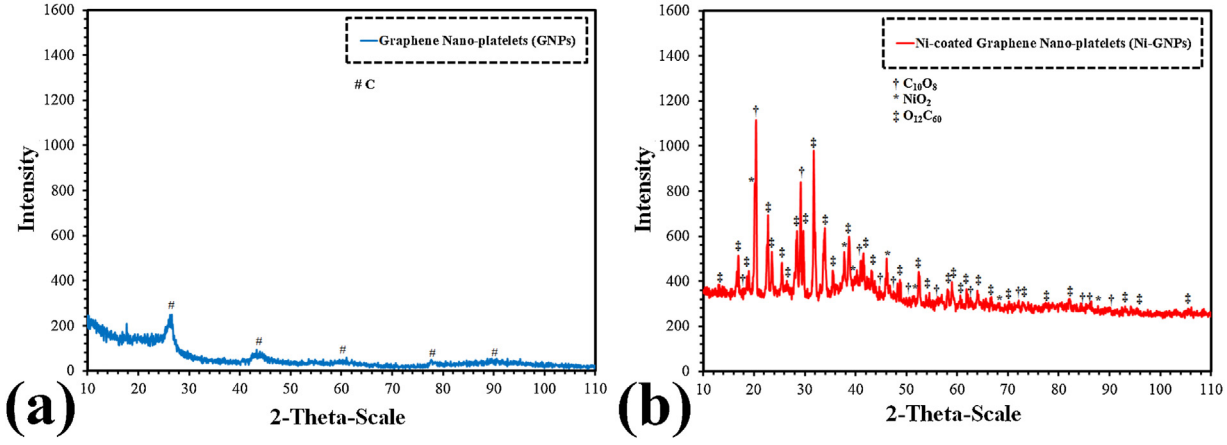

Fig. 2 – XRD patterns of GNPs (a) before and (b) after Ni-coating.

influence of GNPs content in terms of changing in the weight fraction, (ii) Ni-coating modification of GNPs by electroless plating, and (iii) optimizing the isothermal aging treatment in terms of temperature and time control. Considering the influence of intermetallic compounds (IMCs) as reinforcing hard particles through the solder alloy matrix and as a chemical bonding layer at the interface with the copper substrate on the mechanical performance of soldered joints [53,54], alterations in the formation and growth of IMC particles and layers were studied in more details by controlling the main

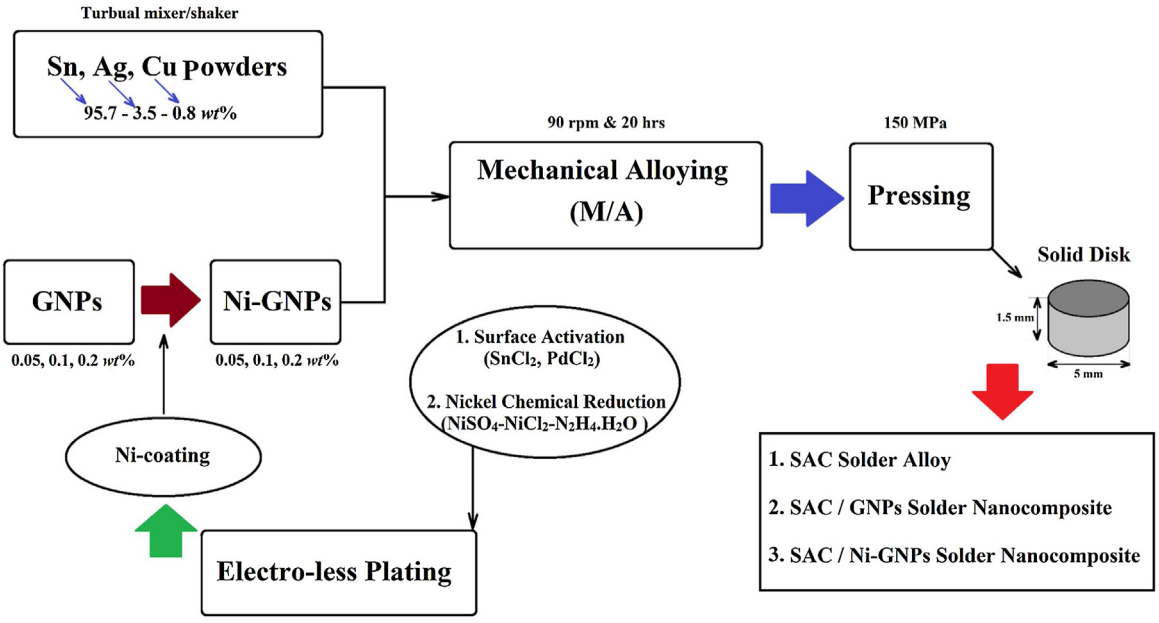

Fig. 3 – Schematic representation of the accomplished procedure for the fabrication of nanocomposite solders.

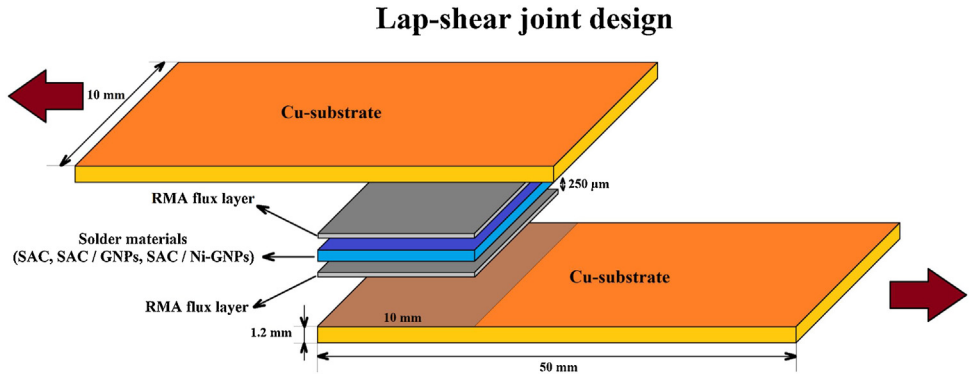

Fig. 4 – Schematic of soldering procedure.

soldering parameters. To this end, depending on the change in the content of GNPs (in the range of 0–0.2 wt%), employing of Ni-coating for modification of the surface of GNPs, and implementation of isothermal aging treatment, a correlation was established between the microstructural details and mechanical properties to reach the maximum joining efficiency.

2. Materials and methods

2.1. *Raw materials*

In this work, elemental powders of tin (Sn), silver (Ag), and copper (Cu) with chemical purity and characteristics, as expressed in Table 1, were supplied from the Merck Company (Germany) and utilized to prepare the solder alloy. Furthermore, graphene nanoplatelets (GNPs) with a diameter of <2 μm, thickness of <20 nm, and high purity, as shown in Table 1, were purchased from the US Nano Company (USA) and used as the secondary phase reinforcing agent. High magnification bright- and dark-field transmission electron microscopy (TEM) images and selected area diffraction (SAD) patterns from these GNPs are illustrated in Fig. 1a–c, respectively.

2.2. *Electroless deposition of nickel on the graphene surface*

As one of the main interests of the present research, some portion of GNPs was coated with nickel before application. As previously mentioned, the role of this Ni-coating layer is the reduction of the metallurgical incompatibility between the carbon-based structure of graphene and solder alloy [55]. For a successful decoration of nickel particles on the surface of graphene, the electroless plating technique was employed. At first, a solution containing $SnCl_2$ (10 g/L) and $PdCl_2$ (0.5 g/L) was used to activate the surface of GNPs. For this purpose, GNPs were introduced into the chemical solution and subjected to ultrasonic vibrations for about 30 min to break the aggregates of particles and adequately accomplish the sensitization process. Then, by using a centrifugal

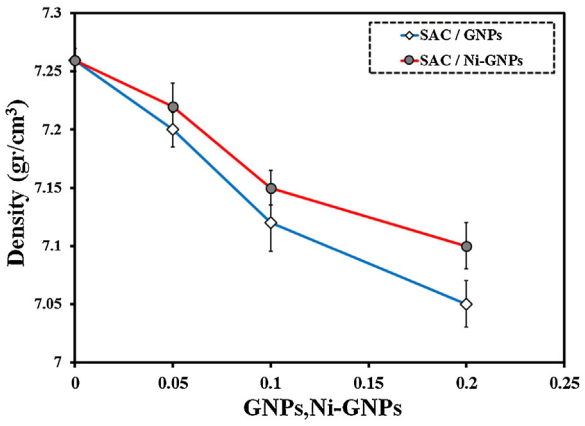

Fig. 5 – The density of solders as a function GNPs content before and after Ni-coating.

system working at a rotational speed of 4000 rpm, the activated GNPs were separated from the solution. After that, the chemical solution for conducting the electroless plating process containing nickel sulfate ($NiSO_4 \cdot 7H_2O$, 25 g/L), hydrazine monohydrate ($N_2H_4 \cdot H_2O$, 30 g/L), sodium tartrate ($C_4H_4O_6Na_2$, 10 g/L), ammonium sulfate ($(NH_4) \cdot 2SO_4$, 50 g/L), and ammonium hydroxide ($NH_3 \cdot H_2O$, 5%), was prepared. By inserting the activated GNPs into the mentioned bath and setting the main parameters for plating, the electroless decoration of nickel particles was successfully carried out. In this regard, the pH of 10, solution temperature of 90 °C, ultrasonic power of 100 W, and the storage time of 45 min were applied as the leading environmental conditions. Toward the direction of chemical reactions and nickel decoration of the surface of graphene, $NiSO_4$ can act as the source of nickel and $N_2H_4 \cdot H_2O$ as a reducing agent. After electroless plating, the Ni-coated GNPs were removed from the solution by using a centrifugal separating system and after that wholly dried in an oven at a temperature of 50 °C for about 24 h. The morphology of Ni-coated GNPs was studied by TEM analysis, and the results are presented in Fig. 1d–f. According to the TEM images in Fig. 1d and e, and diffraction analysis in Fig. 1f, no considerable alteration in the morphology of nanoplatelets during electroless plating can be noted, despite nickel particles decoration on the surface of them. Furthermore, the successful implementation of the Ni-coating process is displayed in the X-ray diffraction (XRD) analysis results of the GNPs before and after Ni-coating in Fig. 2, showing a considerable change in the crystallography of the material and appearance of the peaks corresponding to the Ni-reach compounds. In the following, both of non-coated and Ni-coated GNPs were considered as reinforcing

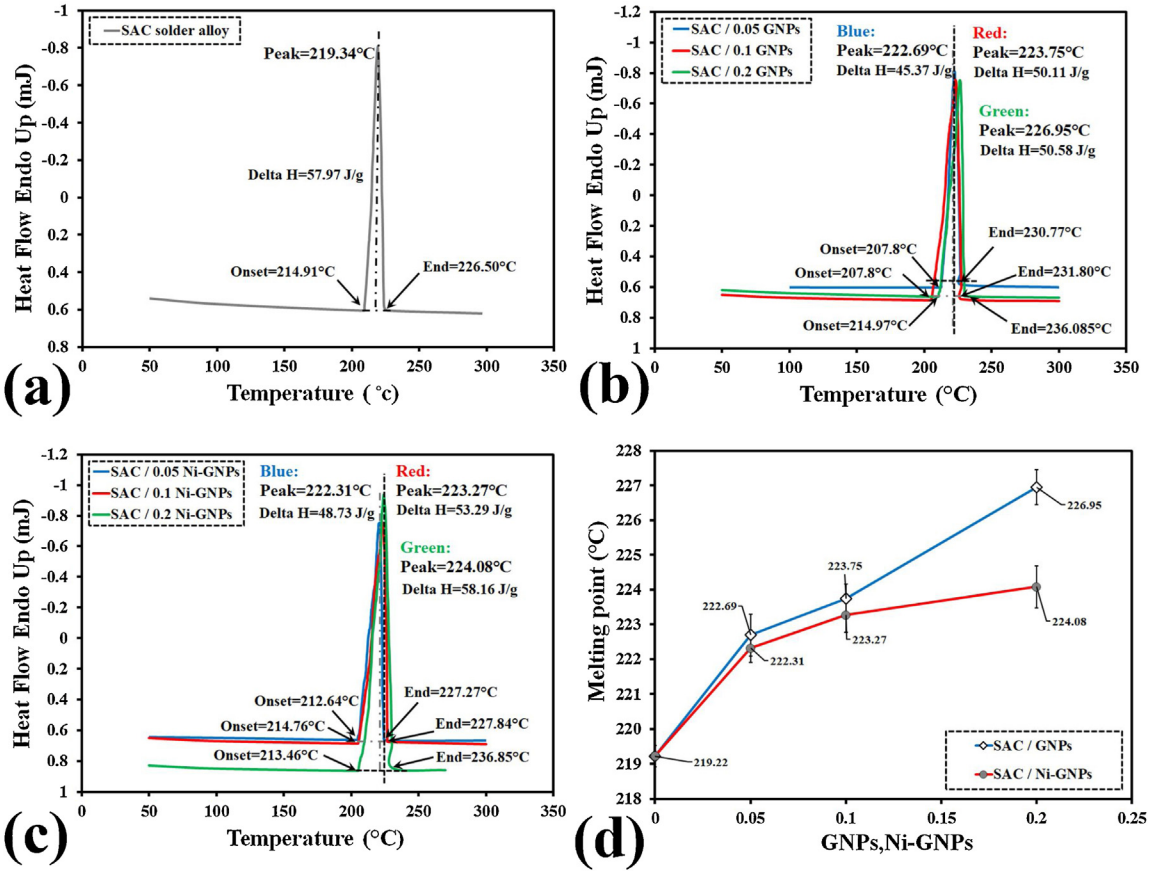

Fig. 6 – DSC heat-flow curves for (a) SAC solder alloy, (b) SAC/GNPs, and (c) SAC/Ni-GNPs solder nanocomposites. (d) The measured melting temperature for different solders versus the content of GNPs before and after Ni-coating based on the presented DSC curves.

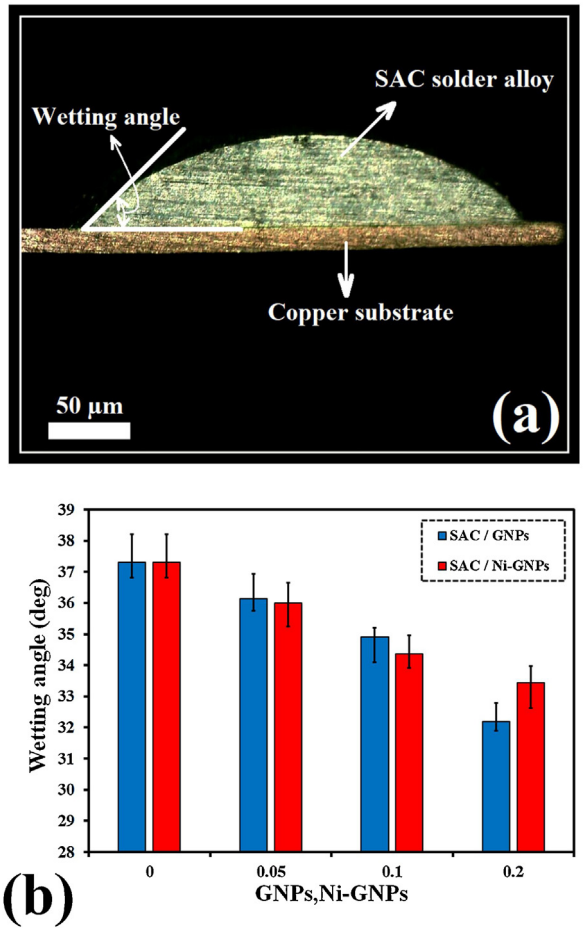

Fig. 7 – (a) Cross-section of soldered joint for assessment of wettability and (b) the measured wetting angle for produced solders as a function of GNPs fraction before and after Ni-coating.

agents to elaborate on the influence of GNPs and Ni-coating, separately.

2.3. *Production of nanocomposite solders*

At first, the Sn, Ag, and Cu elemental powders were mixed according to the eutectic weight percent ratio of 95.8–3.5–0.7 (wt%) by using a simple mixer. Then, GNPs with different weight percent ratios of 0%, 0.05%, 0.1%, and 0.2% were added to the powder mixture of SAC solder alloy. To avoid segregation of elements during soldering induced melting because of difference in the density of ingredients, processing was implemented according to the powder metallurgy (P/M), and mechanical alloying (M/A) routes by using a planetary ball mill. The ball milling process was conducted by setting a rotational speed of 90 rpm for 20 h under the argon atmosphere. To avoid exposing the mixed powders with impurities during the mechanical milling process, the cup and steel balls were made of hard steel coated by chromium. Mixing of all elemental powders was performed under the inert gas atmosphere using argon. After mixing and alloying, the powders were compacted to the small solid disks with a diameter of 5 mm and a thickness of 1.5 mm by placing them into a cylindrical die made of hard steel and applying a uniaxial pressure of 150 MPa. After that, the final sintering step was performed by furnace heating at a temperature of ~185 °C for 2 h under the inert atmosphere using argon gas. Different actions for the preparation of lead-free nanocomposite solders are plotted in the schematic representation of Fig. 3. According to this explained powder metallurgy procedure, the solder alloy and the nanocomposite materials were prepared.

2.4. *Physical properties of the produced nanocomposite solders*

2.4.1. *Density*

To measure the density of compressed and sintered solid disks from the SAC solder alloy and SAC-GNPs nanocomposite solders, the Archimedes method was employed [56]. At first, the weight of samples was measured by a scale. Then, by immersing through the distilled water, the change of the volume was determined. After that, by using the Archimedes equation, density was calculated. For each sample and processing condition, at least three measurements were performed to check the repeatability of data.

2.4.2. *Melting point*

To determine the melting temperature of solder alloy and nanocomposites, differential scanning calorimetry (DSC) analysis was implemented according to the standard of ASTM D3418/E1356. In this regard, a Mettler Toledo DSC instrument (Mettler-Toledo Inc., Canada) was used. For DSC testing, the weight of samples was in the range of 50–70 mg. All tests were conducted under the argon atmosphere with a heating rate of ~10 °C/min up to a maximum temperature of ~300 °C. By observation of a prominent endothermic peak in the heating cycle, the melting temperature was determined. For such melting temperature measurements, also DSC analysis was repeated at least three times, and the average measured data is reported.

2.4.3. *Wettability*

Wettability is a fundamental and determinative physical property of solder materials that can be defined and expressed in terms of the wetting angle. According to designations for the standard of ASTM D7334-08, the contact angle between the copper substrate and different solder materials was measured and compared. In this case, a semi-soldering thermal cycle was accomplished. For such purpose, the solder material and the RMA flux were placed on the polished surface of a copper substrate and then heated up to a maximum temperature of ~250 °C for a holding time of around 5 min in an atmosphere-controlled furnace. After cooling down to the ambient temperature, the set-up was removed from the furnace and sectioned in the middle of a solidified droplet. Then, by using a goniometer equipped camera system, the maximum height and contact angle were measured. For each condition, tests were repeated three times to measure and report reliable data for the wetting angle.

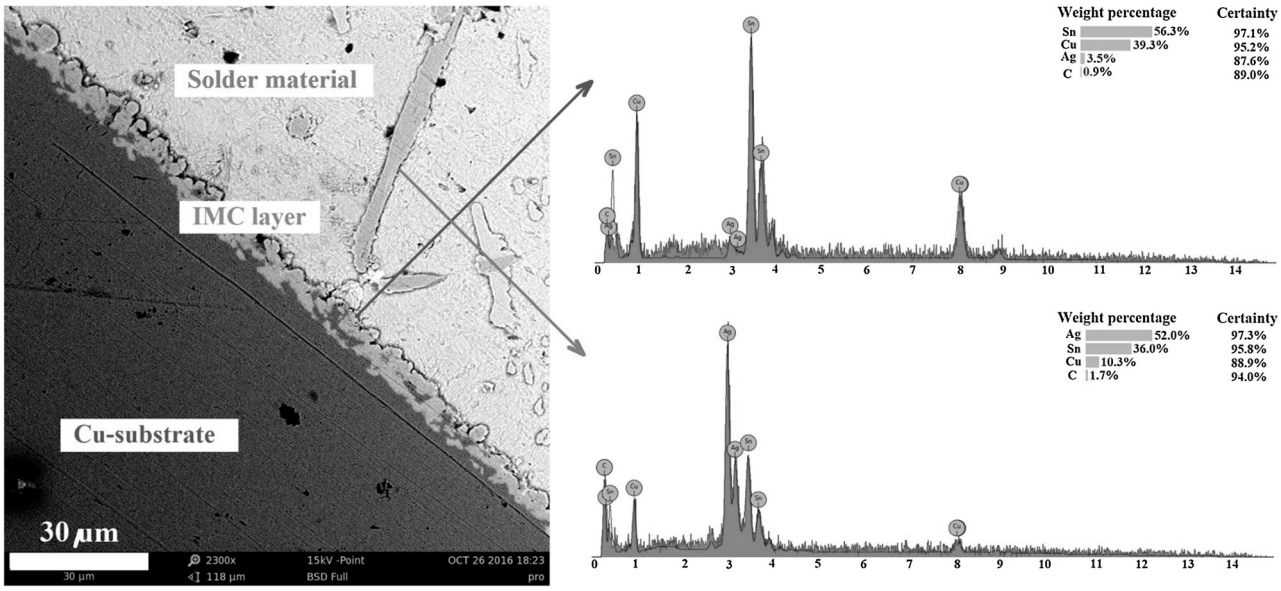

Fig. 8 – The microstructure of Cu/SAC/Cu soldered joint, and the related point-scan EDS analysis results from the IMC layer at the interface.

2.5. *Nanocomposite soldering*

A schematic of the lap shear sample design used for the determination of the mechanical properties of the lead-free nanocomposite solders of this research is illustrated in Fig. 4. Sample preparation for soldering was performed according to the standard of ASTM D1002-94. In this case, square copper sheets with an overlap dimension of 10 mm × 10 mm, a thickness of 1.2 mm, and a length of 50 mm were used. Before conducting the soldering process, the surfaces of copper sheets were ground, polished, and cleaned. With the aid of rolling process and occurrence of dynamic softening of the SAC solder alloy at room temperature, thin foils with a thickness of about 250 μm were prepared and cut to rectangular pieces of 10 mm × 10 mm. After cleaning of the copper substrates and solder foils in an ultrasonic bath of acetone, the RMA flux was pre-placed at the interface between the substrate and solder to avoid undesirable oxidation and also aid the deoxidizing process. As it is well established, the RMA flux, which is a synonym for mildly activated rosin, contains the volatile acids that can react with the oxide layers on the surface of the substrates and, therefore, aid cleaning the surface before soldering [1]. Furthermore, by covering the soldering area like a slag layer, it can avoid any undesirable oxidation during the soldering process [1]. Then, the lap-shear sample was placed as a sandwich within a soldering fixture with the desired amount of pressure loading. The final soldering step was performed by placing this set-up into an atmosphere-controlled furnace, heating up to the maximum temperature of 250 °C, holding for 30 min, and then cooling down to the room temperature. This soldering process was carried out for the SAC solder alloy as well as all SAC-GNPs nanocomposite solders.

2.6. *Aging treatment*

In order to study the evolution of the microstructure and the mechanical properties of Cu/SAC/Cu and Cu/SAC-GNPs/Cu soldered joints, isothermal aging treatment was performed. This post-processing was performed by placing the soldered joints in the furnace at the temperature of ~150 °C and holding up to long times as 100 h. Subsequently, the samples were removed from the oven and cooled down to room temperature.

2.7. *Characterization of the soldered joints before and after aging*

2.7.1. *Microstructural analysis*

Microstructural studies were performed across the thickness section of the soldered joints before and after isothermal aging treatment. For this purpose, the prepared lap-shear joints were cross-sectioned by using a diamond cutter and considered for further metallographic sample preparation. After the accomplishment of standard mechanical grinding and polishing, a chemical reagent made of 2 vol% HCl and 2 vol% HNO_3 through the ethanol solution (96 vol%) was used to reveal the grain structure of solder matrix. After that, the microstructure of samples was analyzed using field emission-scanning electron microscopy (FE-SEM). A JEOL 7600F FE-SEM microscope (JEOL, Japan) equipped with the energy-dispersive X-ray spectroscopy (EDS) detector was used for these analyses.

2.7.2. *Transverse (tensile)-shear testing*

To evaluate the mechanical properties of non-aged and aged lap shear solder joints prepared with SAC solder and SAC-GNPs nanocomposite solders before and after Ni-coating, shear testing was conducted in accordance with the standard of ASTM D1002. In this regard, a SANTAM uniaxial universal tensile loading machine (SANTAM STM150, Iran) was used. All shear tests were performed at room temperature with setting

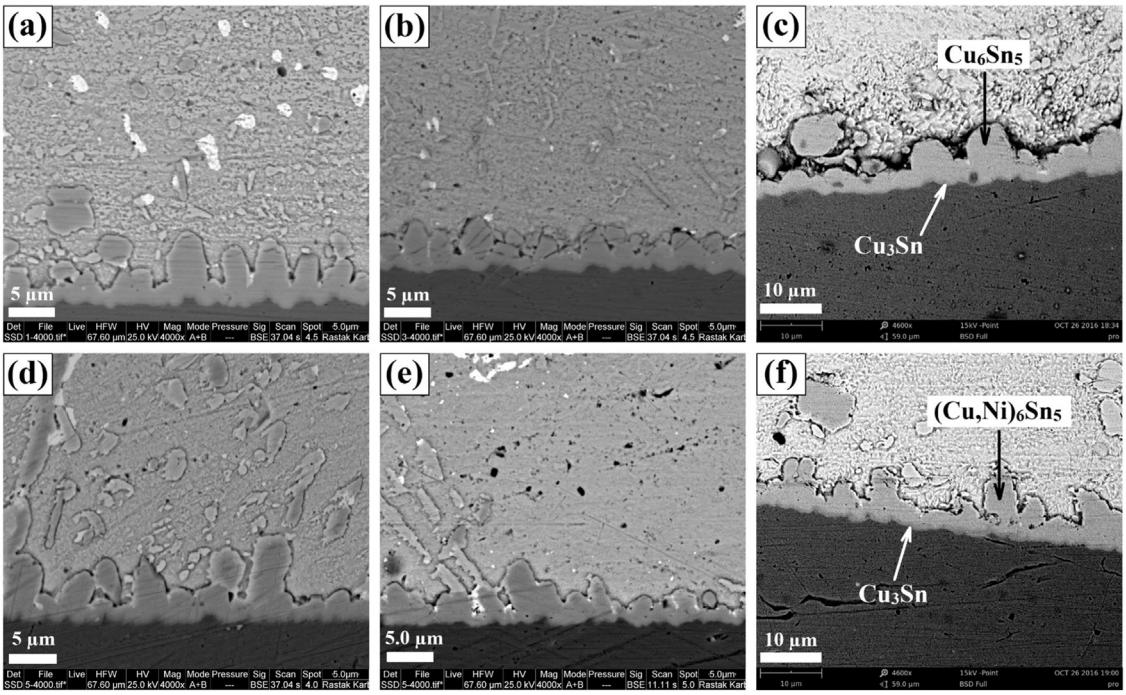

Fig. 9 – Microstructure of soldered joints reinforced by (a, d) 0.05, (b, e) 0.1, and (c, f) 0.2 wt% GNPs (a–c) before and (d–f) after nickel coating.

a constant cross-head speed of 2 mm/min. For each processing condition, experiments were repeated three times, and the average mechanical properties in terms of shear strength and flexibility were calculated and reported.

2.7.3. *Fracture behavior*

After shear testing, the fracture surfaces of the non-aged and aged soldered joints were evaluated by visual examination of the failed components. To study the failure behavior of the samples with more details, fractographic investigations were conducted utilizing FE-SEM.

3. Results and discussion

3.1. *Effects of GNPs and Ni-coating on the physical properties of solders*

3.1.1. *Density*

The measured density results for SAC-GNPs nanocomposite solders before and after nickel electroless coating are plotted in Fig. 5 versus the content of GNP compared to the un-reinforced SAC solder alloy. Considering the theoretical density for SAC solder alloy of ~7.40 g/cm^3, a density of ~98% of the theoretical value is attained after the implemented processing route in this work according to P/M and M/A. By solder nanocomposite fabrication and increasing the amount of reinforced GNPs up to ~0.2 wt%, density is continuously reduced down to ~95% of the theoretical value. Such a trend could be attributed to an increase in the resistance of the powder mixture to compaction with increasing the amount of the reinforcing agent. Although in the presence of Ni-coating, a slightly lower density reduction can be noted caused by enhancing the compatibility between the graphene and solder alloy matrix [48,57,58].

3.1.2. *Melting temperature*

The DSC testing results as heat flow curves for first solder alloy and nanocomposite solders are demonstrated in Fig. 6a–c. The results for the melting point of solder alloy and nanocomposites measured by DSC analysis before and after Ni-coating as a function of GNPs content are summarized in the graph of Fig. 6d. As seen, by increasing the amount of incorporated GNPs, the melting temperature of solder is continuously increased. A maximum temperature rising of ~5–8 °C can be noted after introducing of GNPs with the content of ~0.2 wt% in contrast to the melting temperature of ~219.2 °C for SAC solder alloy. Meanwhile, in the presence of Ni-coating, alteration in the melting point is not significant as compared to the none-coated ones, i.e., <1–3 °C. In general, change of melting temperature in such a minor range maybe ignorable for practical applications. Concerning the variation of melting temperature of the SAC solder alloys in the presence of the reinforcing agent, different reports can be found in the literature [2]. Depending on the type of secondary phase reinforcing nano-sized agents, in some cases, a slight increase, in some instances, slightly decreasing, and in some others, no alteration of melting temperature for SAC-based nanocomposite solders was highlighted [2]. However, the results of the present research illustrate a slight increase in the melting point of the solder due to the addition of GNPs to the SAC solder alloy matrix.

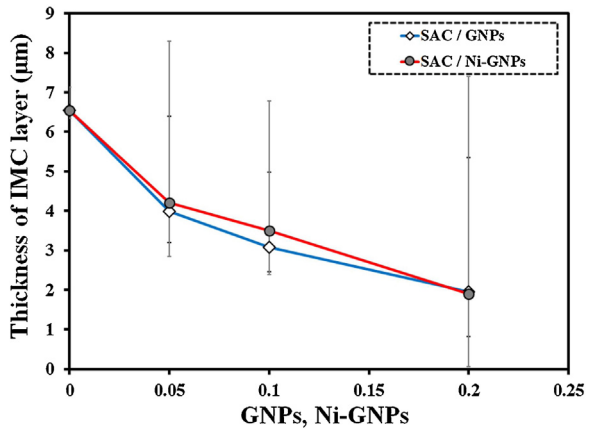

Fig. 10 – Variations of IMC layer thickness versus the content of GNPs without and with nickel coating immediately after soldering.

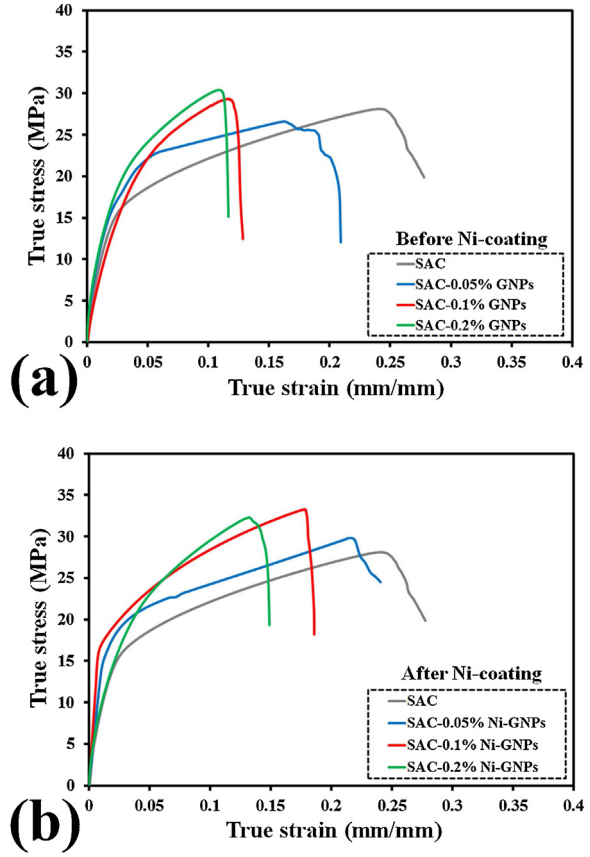

Fig. 11 – Tensile-shear flow behavior of the soldered joints by reinforcing different contents of GNPs (a) before and (b) after Ni-coating.

3.1.3. *Wetting angle*

The wetting angle for first solder alloy and processed nanocomposite solders was determined based on a cross-sectional examination of the soldered samples, as shown in Fig. 7a. In Fig. 7b, the wettability of solder nanocomposites is compared with the SAC solder alloy in terms of the wetting

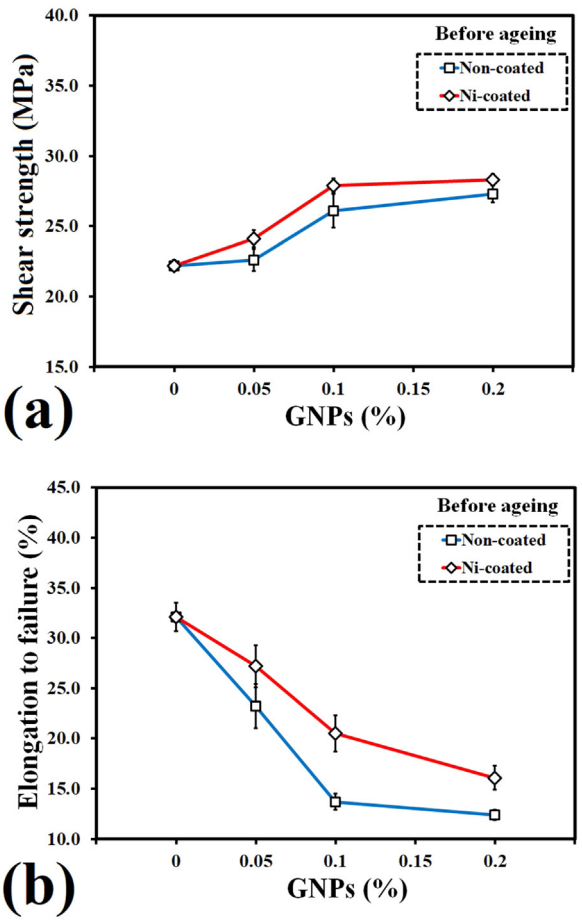

Fig. 12 – Effects of non-coated and Ni-coated GNPs on (a) shear strength and (b) elongation to failure of the soldered joints.

angle. In this regard, the lower wetting angle corresponds to a better wettability. The results reveal the beneficial influence of GNPs with a continuous decrease in the wetting angle with increasing the GNPs content in all cases. A maximum wetting angle decrease of about 5 degrees is attained by incorporation ~0.2 wt% of GNPs.

Based on data presented in Figs. 5–7, incorporation of GNPs and the presence of Ni-coating leads to a continuous increase in the melting temperature of solder as well as a constant decreasing trend in the density and wetting angle. It is worth noting that graphene cannot react with the molten solder alloy during the mechanical milling, subsequent reflow processes, and even during service conditions [48]. However, incorporation of these GNPs as a secondary phase can retard the melting process by acting as a hindering agent, which consequently leads to a slight increase in the melting temperature. Also, they can improve the wettability on the copper substrate during the reflow process in terms of decreasing the wetting angle caused by accelerating the diffusion phenomena and chemical reactions at the interface due to higher configurational entropy [45,59].

Table 2 – Mechanical properties of soldered joints reinforced by different contents of GNPs and Ni-GNPs.

Solder	Composition	Modification	Content of GNPs (wt%)	E (GPa)	τ_Y (MPa)	τ_{UTS} (MPa)	τ_F (MPa)	e (%)
Alloy	SAC	–	0	45.6	14.8	22.2	15.1	32.1
Nanocomposite	SAC-GNPs	–	0.05	47.5	17.8	22.6	9.8	23.2
Nanocomposite	SAC-GNPs	Ni-coating	0.05	48.1	16.2	24.1	19.3	27.2
Nanocomposite	SAC-GNPs	–	0.1	49.4	18.8	26.1	10.9	13.7
Nanocomposite	SAC-GNPs	Ni-coating	0.1	50.1	16.5	27.9	15.1	20.5
Nanocomposite	SAC-GNPs	–	0.2	52.5	19.2	27.3	13.5	12.4
Nanocomposite	SAC-GNPs	Ni-coating	0.2	53.4	19.4	28.3	16.7	16.1

* E, elastic modulus; τ_Y, yield stress; τ_{UTS}, ultimate shear strength; τ_F, fracture stress; e, elongation to failure.

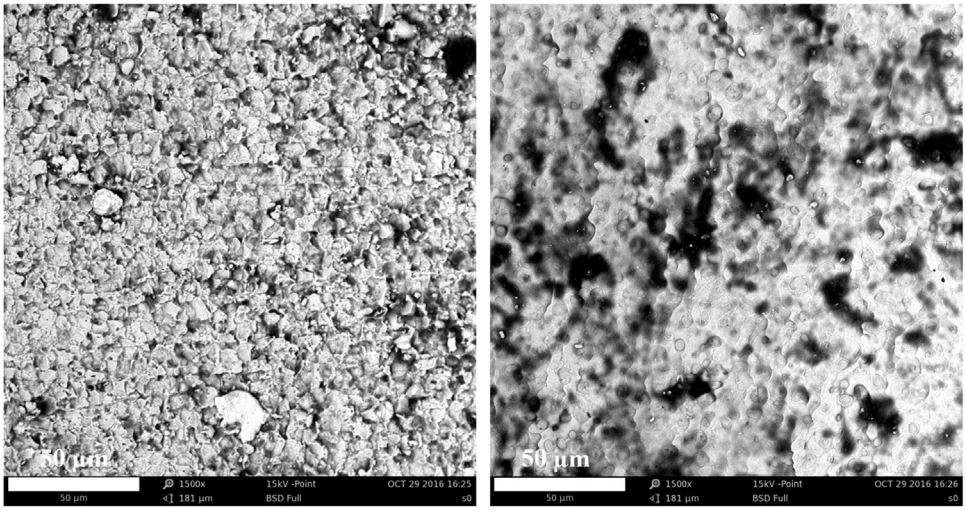

Fig. 13 – FE-SEM images from the fracture surface of a failed Cu/SAC/Cu soldered joint.

3.1.4. *Microstructure*

FE-SEM images showing the microstructural features for processed solder alloy and nanocomposites are presented in Supplementary Electronic Document, ESI Fig. S1. The effects of GNPs content and Ni-coating modification on the grain structure of the SAC solder alloy matrix can be found by comparing these micrographs. Moreover, the distribution of intermetallic compound (IMC) particles through the solder alloy matrix are noted as the large and elongated secondary phases along the grain boundaries. According to the composition of SAC alloy, these particles are mainly consisting of Ag_3Sn intermetallic phase after solid-state processing via P/M and M/A routes of manufacturing. By increasing the weight fraction of GNPs, the grain structure of solder alloy becomes continuously finer (compare ESI Fig. S1a–S1c). In this case, the average grain size was reduced from an initial value of ~50 μm for SAC alloy down to ~20 μm for SAC-GNPs nanocomposite after incorporation of ~0.2 wt% GNPs. Also, the distribution of IMC particles develops as homogenous and with finer sizes. Further microstructural refinement (~15 μm) and more uniform dispersion of IMC particles are attained by utilizing the Ni-coated GNP as a reinforcing agent in 0.2 wt% (see ESI Fig. S1d). Continuous refining the microstructure of solder alloy by introducing the GNPs into the SAC solder alloy matrix and increasing its content (as shown in ESI Fig. S1) could be attributed to the pinning action of nanoplatelets against the operative dynamic restoration phenomena during P/M and M/A processing routes [51,57]. Attaining a uniform dispersion from these phases is provided by increasing the content of GNPs, as illustrated in FE-SEM micrographs of ESI Fig. S1.

3.2. *Effects of GNPs and Ni-coating on the microstructure and mechanical properties of soldered joints*

3.2.1. *Microstructure*

The cross-sectional micrographs of copper soldered joint by using SAC solder alloy is shown in the FE-SEM image of Fig. 8. According to this micrograph, the formation of a continuous IMC layer at the interface with the copper substrate and several distinct elongated IMC particles through the SAC solder alloy can be noted. The growing morphology of this IMC layer seems like scallop-shaped, with a chemical composition/stoichiometry near to Cu_6Sn_5 phase, and an average thickness of ~4.7 μm. In the presence of GNP as a reinforcing agent within the matrix of solder alloy, different microstructural aspects can be seen in FE-SEM images of Fig. 9 before and after Ni-coating depending on the weight fraction of GNPs. At first, the morphology of the IMC layer at the interface changed

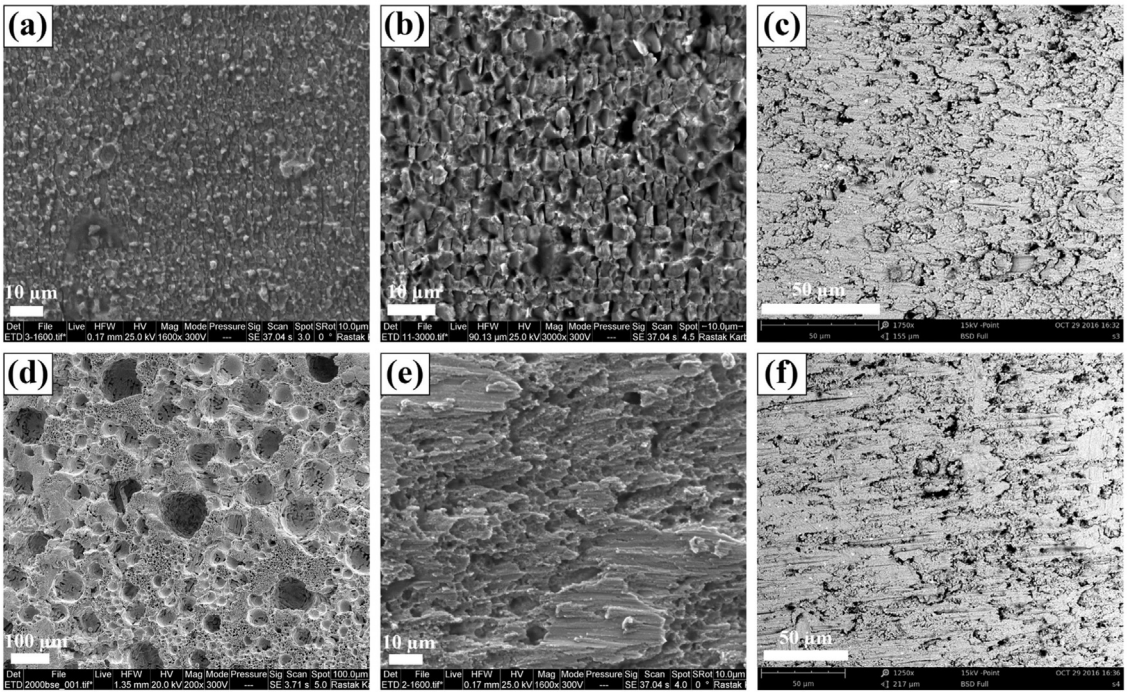

Fig. 14 – FE-SEM images from the solder side fracture surfaces of failed soldered joints modified with (a, d) 0.05, (b, e) 0.1, and (c, f) 0.2 wt% GNPs (a-c) before and (d-f) after nickel coating.

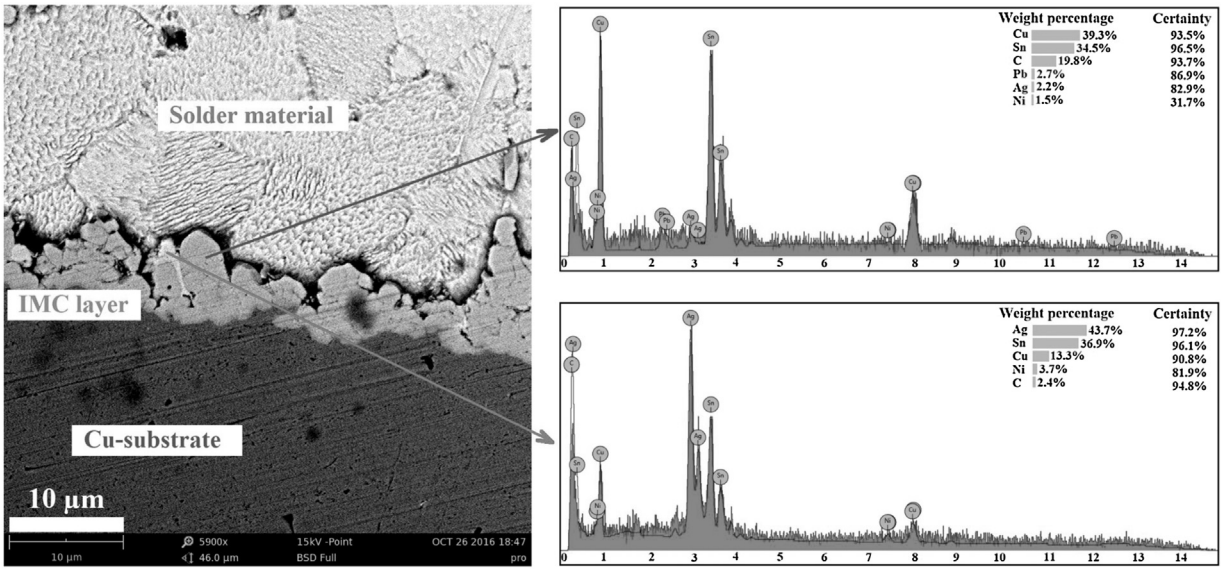

Fig. 15 – Microstructure and EDS analysis of Cu/SAC/Cu soldered joint after aging treatment at 150 °C for 100 h.

from the bar-shaped toward the cauliflower-state. Furthermore, in proportion to the amount of incorporated GNPs, the thickness of the IMC layer is continuously reduced, as shown in Fig. 9a–c. After introducing a 0.2 wt% of reinforcing non-coated GNPs, the mean thickness of ~2.8 μm was attained. Regarding the SAC solder matrix, Cu_6Sn_5 phase with massive and coarse Ag_3Sn intermetallic with needle-like morphologies are still present with some slight modifications compared to the unreinforced soldered joint. The primary influence of Ni-coating on the surface of reinforcing GNPs was in changing the morphology of IMC particles through the SAC solder alloy matrix and chemical composition of the IMC layer at the interface with the copper substrate (see Fig. 9d–f). For Ag_3Sn intermetallic particles inside the SAC solder matrix, the morphology is nearly changed from needle-type into the equiaxed with a more elegant distribution. Moreover, besides improving the compatibility of graphene with the solder alloy, a further important role of nickel is changing the chemistry of the interfacial IMC layer. In the new state, the interface layer with a copper substrate consists of two phases with the different sto-

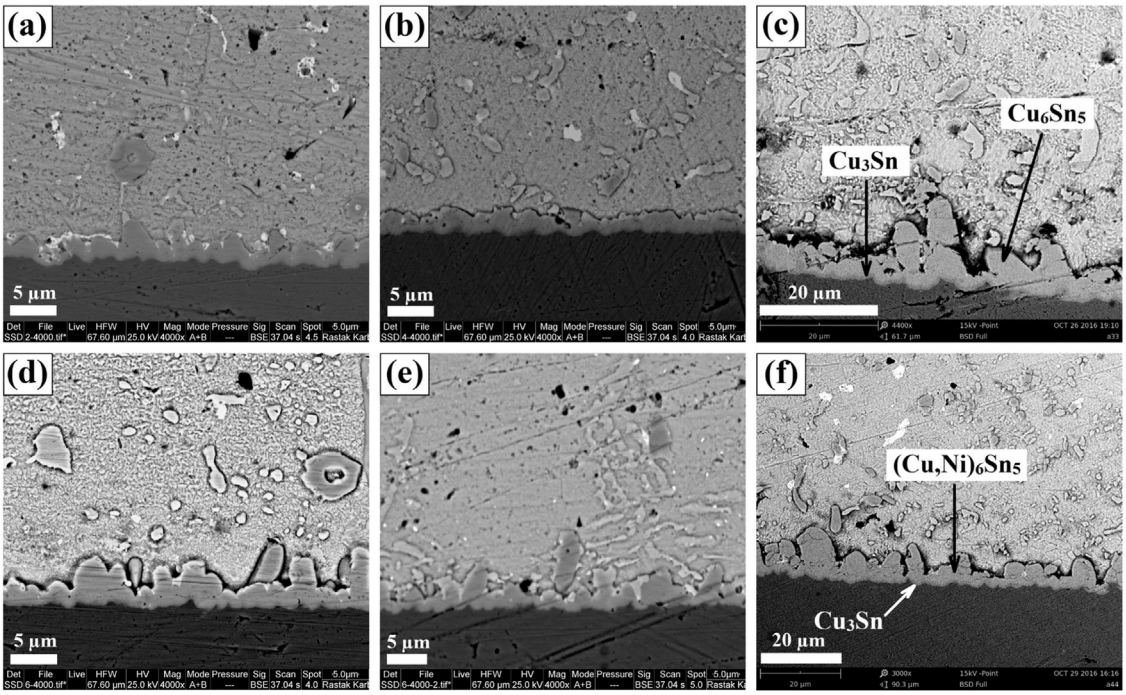

Fig. 16 – Microstructure of nanocomposite soldered joints after aging treatment at a temperature of 150 °C for 100 h; (a–c) 0.05–0.2 wt% GNPs and (d–f) 0.05–0.2 wt% Ni-GNPs.

ichiometry of Cu_3Sn and (Cu, Ni)$_6Sn_5$. Also, the thickness of these layers was increased by the presence of nickel slightly. The effects of GNPs with and without nickel decoration on the average thickness of the IMC layer at the interface are plotted in Fig. 10. In both cases, a decreasing trend can be noted. Although, the slope of reduction was slightly lower in the presence of nickel coating.

During the soldering process, the solder alloy and nanocomposites were reflowed between two sheets of copper, resulting in a change of the microstructure comparing to that induced by P/M and M/A processing routes due to melting and solidification phenomena. Exposing the molten solder alloy and nanocomposite against the copper substrate leads to the occurrence of liquid-solid state chemical reactions and the formation of the IMC layer with a stoichiometry of Cu_6Sn_5 at the interface caused by dissolution of Cu-substrate into the molten solder material [2]. The morphology of the Cu_6Sn_5 phase at the interface with the copper substrate was found scalloped during the reflow process (see Figs. 8 and 9). This Cu_6Sn_5 phase is well-known as η in Cu-Sn soldering systems. However, another stoichiometry with the chemical composition of Cu_3Sn, named as ε phase, has the chance of formation, as well. According to the reported data in the literature [27], the driving force of η phase formation is considerably higher with a lower kinetic barrier. Meanwhile, its alteration to form the ε phase needs to overcome significantly higher activation energy. In general, the increased diffusion rate of Cu element by increasing temperature and time of the reflow process leads to thickening of η phase layer with a scallop type morphology and formation of ε phase after a specific incubation time [27,60]. However, in the presence of Ni as a coating material on the surface of GNPs, it can rapidly diffuse into the Cu-substrate interstitially. This second reaction can change the chemistry of the IMC layer to a more stable ternary phase compound of (Cu, Ni)$_6Sn_5$. Although, the primary effect of GNPs is on suppressing the kinetics of IMC layer growth by retarding the migration of solidification edge.

3.2.2. *Shear properties*

The real stress-strain curves for the lap-joints before and after Ni-coating are demonstrated in Fig. 11a and b, respectively. Also, the effects of GNPs incorporation, its content, and Ni-coating modification on the main shear properties of soldered joints are expressed in Table 2. The influence of non-coated and Ni-coated GNPs with different substances on the shear strength and flexibility of the soldered joints is illustrated in Fig. 12a and b, respectively. Based on these flow curves, three main issues can be highlighted, as follow; (i) incorporation of GNPs displayed a considerable influence on improving the shear strength even though some elongation loss, (ii) increasing the amount of GNPs up to 0.2 wt% leads to continuous enhancement of shear strength, and (iii) Ni-coating modification exhibited very effective in keeping the elongation to failure with a higher increase of strength [61,62]. Concerning the SAC solder alloy with a shear strength of ~22.2 MPa and a ductility of ~32.1%, by simultaneous employing of GNPs as reinforcing agent and Ni-coating modification, the highest strength of ~28.3 MPa is attained for solder nanocomposite with the ductility of ~16.1%. Therefore, a maximum shear strength enhancement ratio of ~27.5% can be noted. On the other side, without Ni-coating, incorporation

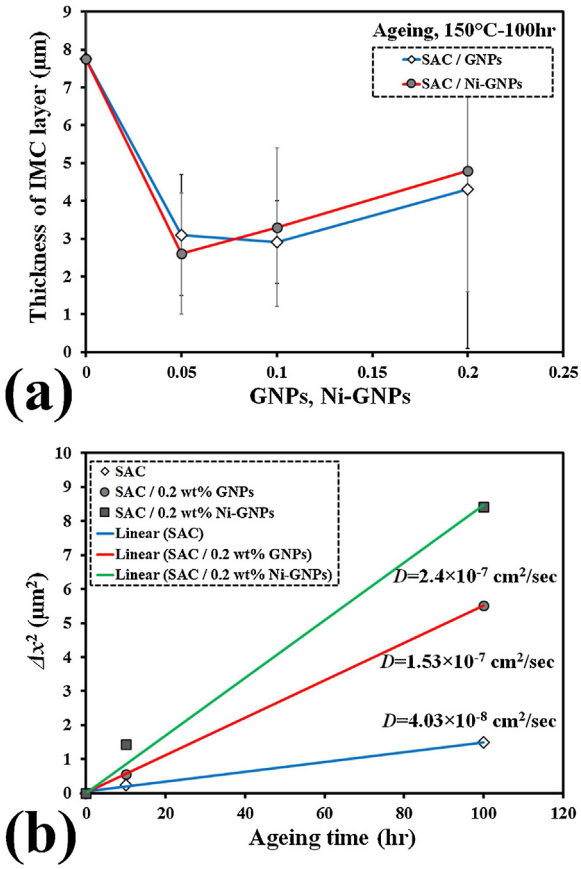

Fig. 17 – (a) The average thickness of the IMC layer at the interface versus the content of reinforcing GNPs after aging treatment at a temperature of 150 °C for 100 h. (b) Variations of IMC layer thickness square versus the aging time to determine the inter-diffusion coefficient.

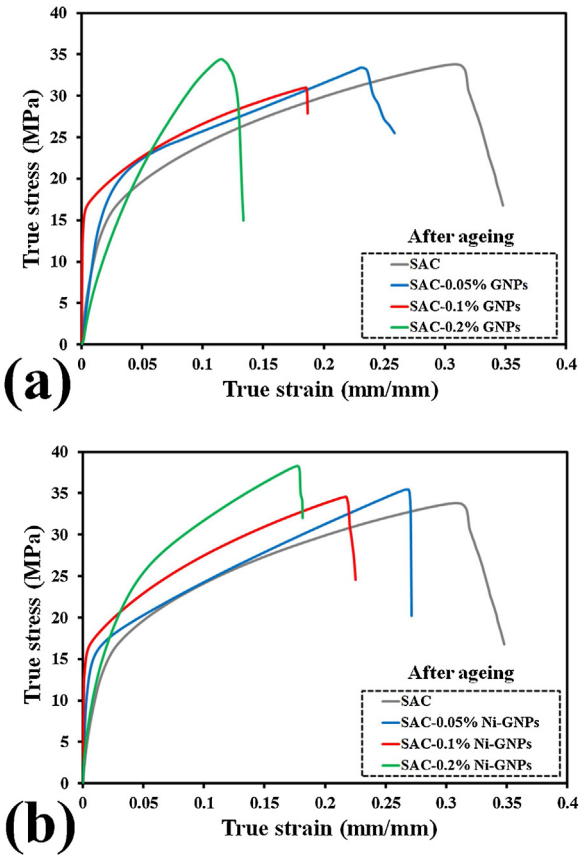

Fig. 18 – Tensile-shear flow behavior of the soldered joints after aging treatment at a temperature of 150 °C for 100 h in the presence of GNPs (a) without and (b) with Ni-coating.

of GNPs up to a weight fraction of 0.2% leads to a shear strength increase of ~27.3 MPa with a minimum ductility of ~12.4%.

3.2.3. *Fractographic aspects*

All soldered joints failed either within the soldered area or along with the interface between the continuous IMC layer and solder material. By using GNPs as the reinforcing agent in the form of non-coated or Ni-coated, the failure behavior was changed from the IMC control mode to the solder control mode, in contrast to the interfacial controlling mechanism for SAC solder alloy. FE-SEM fractography for the fracture surfaces related to the Cu/SAC/Cu soldered joint is shown in Fig. 13. Fig. 14 illustrates the FE-SEM micrographs from the fracture surfaces of the nanocomposite soldered joints with different contents of GNPs before and after Ni-coating. As seen, by increasing the content of GNPs, the fracture surface roughness is increased, showing the failure mode changing from IMC control to solder control. On the other hand, by introducing the GNPs and reinforcing the SAC solder matrix, it becomes more brittle, and cracks path can be changed toward the solder material instead of following the IMC layer at the interface. Moreover, different fractographic features before and after Ni-coating can be noted (compare Fig. 14a–c and d–f), and it seems that in the presence of Ni-coating, the fracture behavior tends to be more ductile by showing more shear or dimple-like features on the fracture surface.

3.3. *Effects of aging treatment on the microstructure and mechanical properties of the soldered joints*

3.3.1. *Microstructure*

Cross-sectional FE-SEM microstructure and EDS analysis results for the Cu/SAC/Cu soldered joint after aging treatment at a temperature of 150 °C for 100 h are shown in Fig. 15. As evident, the thickness and composition of the IMC layer at the interface considerably changed after aging treatment. With a thickening up to the range of ~8.4–13.0 μm, the morphology of the IMC layer altered to the irregular columns. Furthermore, the composition of the IMC layer changed as well, and the chemistry of this interfacial reaction zone tended toward a different stoichiometry of Cu_3Sn, caused by accelerating the solid-state inter-diffusion of Cu and Sn elements during aging treatment. Moreover, a new Ag_3Sn IMC layer formed partially on the Cu_6Sn_5 IMC layer. In Fig. 16, the cross-sectional micrographs of solder joints with nanocomposite solders reinforced by GNPs before and after Ni-coating are demonstrated. Concerning the SAC solder alloy in Fig. 15, less thickening of the IMC layer can be noted, although this growth phe-

Table 3 – Mechanical properties of soldered joints after post-aging treatment at a temperature of 150 °C for 100 h.

Solder material	Modification	E (GPa)	τ_Y (MPa)	τ_{UTS} (MPa)	τ_F (MPa)	e (%)
SAC alloy	–	46.1	15.9	25.0	11.8	41.2
SAC/0.05% GNPs nanocomposite	Before Ni-coating	48.8	18.7	26.5	19.7	29.5
SAC/0.1% GNPs nanocomposite	Before Ni-coating	49.0	16.5	25.8	23.1	20.5
SAC/0.2% GNPs nanocomposite	Before Ni-coating	51.2	21.1	30.7	13.1	14.3
SAC/0.05% Ni-GNPs nanocomposite	After Ni-coating	52.5	15.9	27.2	15.4	31.2
SAC/0.1% Ni-GNPs nanocomposite	After Ni-coating	53.9	16.5	27.9	19.6	25.2
SAC/0.2% Ni-GNPs nanocomposite	After Ni-coating	54.8	23.6	32.1	26.7	19.9

nomenon was mainly temperature control. Despite the lower thickness, the continuity and integrity of the IMC layer at the interface was enhanced in the presence of GNPs as the reinforcing agent. Also, by comparing the matrix of the soldered area between non-coated and Ni-coated GNPs nanocomposite solders in Fig. 16a–c and d–f, it can be emphasized that by increasing the content of GNPs as reinforcing agent from 0.05 to 0.2 wt%, the distribution of Ag_3Sn and Cu_6Sn_5 intermetallic particles through the SAC solder alloy matrix becomes more delicate and more uniform/homogenous, which is further enhanced in the presence of Ni-coating. Fig. 17a shows the alteration of IMC layer thickness as a function of reinforcing agent content for both coated and non-coated conditions after long term aging treatment at a temperature of 150 °C for 100 h. It is evident that under both processing conditions, the thickness of the IMC layer at the interface is considerably changed. Meanwhile, the trend of data evolution is different from Fig. 10. As shown, by increasing the content of GNPs up to 0.05 wt%, the thickness of the IMC layer is decreased, and after that, up to 0.2 wt%, it is continuously increased.

It is well-established that the formation and growth of the IMC layer at the interface of solder material with the copper substrate is a diffusion-controlled phenomenon for the occurrence of the solid-state interfacial chemical reactions [2]. According to a general parabolic equation, as follow, the solid-state kinetics for growth of the IMC layer can be modeled depending on the reaction time (holding time) [63].

$$x_t = \sqrt{\tilde{D}t} \tag{1}$$

In this relationship, x_t is a parameter related to the thickness of the IMC layer at the interface, $\tilde{D}$ is the inter-diffusion coefficient, and t is the solid-state aging time for isothermal aging treatment. The parameter of x_t includes the thickness of the IMC layer immediately after the reflow soldering process plus to its thickening during aging treatment. It is worth to note that the mentioned parabolic equation is satisfied for a layered growth morphology of Cu_6Sn_5 phase at the interface. Where the growth morphology is changed to a scallop-type under the influence of interfacial diffusion/reaction controlled phenomena, the above equation is not adequate anymore, and ripening kinetics according to the below relationship must be employed [2].

$$x_t^3 = \tilde{D}t \tag{2}$$

Since the inter-diffusion phenomenon for different elements controls the formation of IMC layer during the reflow process and its growth kinetics during the solid-state aging

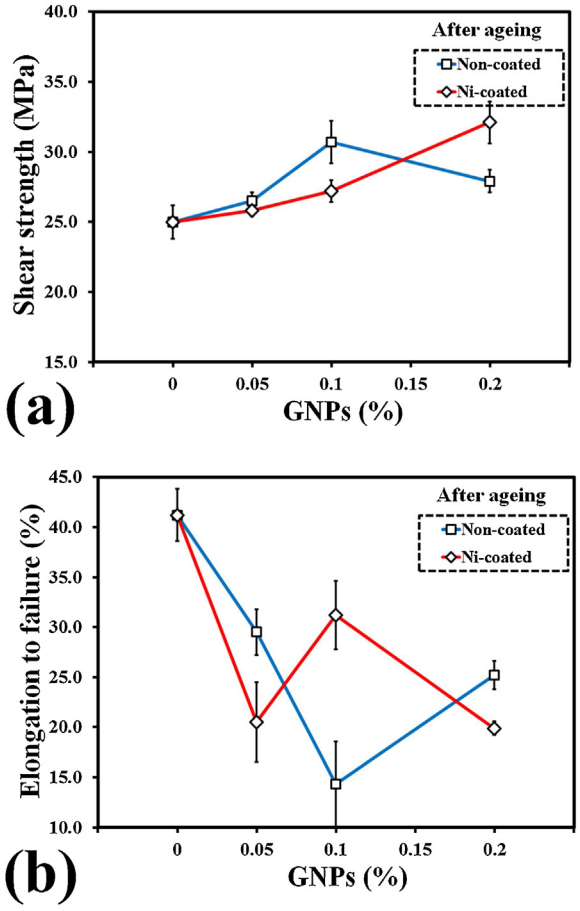

Fig. 19 – Effects of non-coated and Ni-coated GNPs on (a) shear strength and (b) elongation to failure of the soldered joints after aging treatment.

treatment, therefore the diffusion coefficient can be primarily varied as a function of temperature through an Arrhenius relation, as below [64]:

$$\tilde{D} = \tilde{D}_0 \exp\left(-\frac{Q}{kT}\right) \tag{3}$$

where $\tilde{D}_0$ is the pre-exponential inter-diffusion coefficient factor, Q is the activation energy for inter-diffusion of elements, k is the Boltzmann constant, and T is the processing temperature. By combining Eqs. (1) and (3), it would be possible to predict the thickening of the IMC layer during solid-state aging

treatment in terms of the controlling parameters, which are the aging temperature and aging time [2].

$$x_t^2 = \tilde{D}_0 t \exp\left(-\frac{Q}{kT}\right) \quad (4)$$

According to this relationship, the solid-state growth of the IMC layer is more affected by the temperature rather than time. Meanwhile, by the simultaneous increase of the aging temperature and time, the IMC layer becomes massive and denser. Fig. 17b illustrates the variation of IMC layer square thickness as a function of aging time. In contrast, the slope of lines yields the inter-diffusion coefficient for the formation of the IMC layer at the interface. As shown, in the presence of nickel particles as a coating layer on the surface of GNPs, higher inter-diffusion coefficients are determined. Such an effect can be attributed to increasing the configurational entropy in the multi-elements state for the formation of the IMC layer at the interface [2].

On the other side, the phase transformation during the solid-state aging treatment is mostly dependent on the holding time at a given aging temperature (see Figs. 15 and 16). A change in the morphology of the IMC layer at the interface from scallop-shaped into facets is noticeable as well, following a prolonged aging time (compare Figs. 9 and 16). This alteration in the appearance of the IMC layer to planar is because of Cu_3Sn phase formation with dark-gray contrast as a result of solid-state diffusion (see Fig. 9c, f, and c, f). Since the presence of Cu_6Sn_5 phase can limit the inter-diffusion rate of Cu and Sn atoms as the main controlling factor on the solid-state chemical reactions, the formation of Cu_3Sn phase is carried out at the interface with the Cu-substrate [65]. Usually, the aspect of Cu_6Sn_5 is thicker than Cu_3Sn, with more irregular morphology. During aging treatment, by increasing the thickness of the Cu_3Sn phase, the aspect of Cu_6Sn_5 becomes thinner. Also, there are some features related to the formation of Ag_3Sn intermetallic phase next to the IMC layer. Nevertheless, this Ag-rich phase can only form during the reflow soldering process, and it is mainly affected by the peak temperature. The aging treatment, in terms of increasing the holding time, cannot influence the formation of Ag_3Sn phase considerably [27].

3.3.2. *Shear properties*

The effects of aging treatment at a temperature of 150 °C for 100 h on the flow properties of the soldered joints before and after Ni-coating are demonstrated in Fig. 18a and b, respectively. Moreover, the main shear properties are expressed in Table 3. The influence of non-coated and Ni-coated GNPs with different contents on the shear strength and flexibility of the soldered joints is plotted in Fig. 19a and b, respectively. For all samples, a simultaneous enhancement of shear strength and ductility can be noted as compared to the before the aged state. In regards to the SAC solder alloy without any reinforcing agent, elongation to failure is improved more than ~41%. For nanocomposite solders, aging treatment exhibited a more profound influence by increasing the content of GNPs, especially in the presence of Ni-coating. At the extreme state by incorporation of 0.2 wt% Ni-coated GNPs, a nanocomposite soldered joint with a shear strength of ~32.1 MPa and elongation to failure of up to ~19.9% was attained, showing the increasing strength and ductility ratios of ~13.4% and 23.6%, respectively, as compared to the none-aged state. In summary, by simultaneous incorporation of GNPs and Ni-coating as well as optimizing the isothermal aging treatment, an excellent combination of shear strength (~32.1 MPa) and elongation to failure (~19.9%) was attained for the soldered joints. This finding is unique, innovative, and applicable, whereas not reported before in the literature.

3.3.3. *Fractographic aspects*

Exemplary FE-SEM images from the fracture surfaces of some solder joints reinforced with non-coated and Ni-coated GNPs after aging treatment are demonstrated in Fig. 20. In comparison with the fractography before aging treatment in Fig. 14, the fracture surface morphology includes larger shear dimples as a result of higher absorbed energy during the plastic deformation. It seems that by employing the Ni-coating modification, the fracture surface tends to be more ductile with a dimple morphology according to the micro-voids coalescence mechanism, as shown in Fig. 20a–b, d–e. Although, by increasing the content of GNPs, the average dimple size was decreased (compare Fig. 20b, e and c, f). Furthermore, some instances related to catastrophic/cleavage crack propagation along the IMCs layer and particles can be highlighted by white color features on the fractography (e.g., Fig. 20a upper right side).

4. Conclusions

The SAC-GNPs nanocomposite solders were prepared in contrast to the eutectic SAC solder alloy according to the processing routes by powder metallurgy and mechanical alloy. The main focus of this research was on elaborating the influence of GNPs content, Ni-coating modification, and isothermal aging treatment on the solderability of these new materials on the copper substrate and evaluation of the resulting mechanical properties of the soldered joints. The essential conclusions can be summarized as follow:

- By increasing the content of GNPs up to ~0.2 wt%, a reduction of density by ~0.25 g/cm^3, an increase of melting temperature by ~7.7 °C and enhancement of the wetting angle by ~5.0 degree were obtained. In the presence of Ni-coating by electroless decoration, these modifications were more significant.
- Formation of two types of intermetallic compound (IMC) layers at the interface with the copper substrate with different thicknesses and morphologies and the chemical stoichiometry of Cu_3Sn and $(Cu, Ni)_6Sn$ was found very useful in resolving the mechanical performance of soldered joints.
- Increasing the weight fraction of GNPs up to ~0.2% and employing Ni-coating modification displayed considerable influence on changing the composition ratio of the IMC layer toward $(Cu, Ni)_6Sn$ phase as well as suppressing its growth to a thickness layer <2.8 μm. Such an effect can be attributed to the retarding action of nanoplatelets against the propagation of the solidification edge.
- With increasing the content of GNPs up to ~0.2 wt%, the shear strength of solder joints continuously improved up to

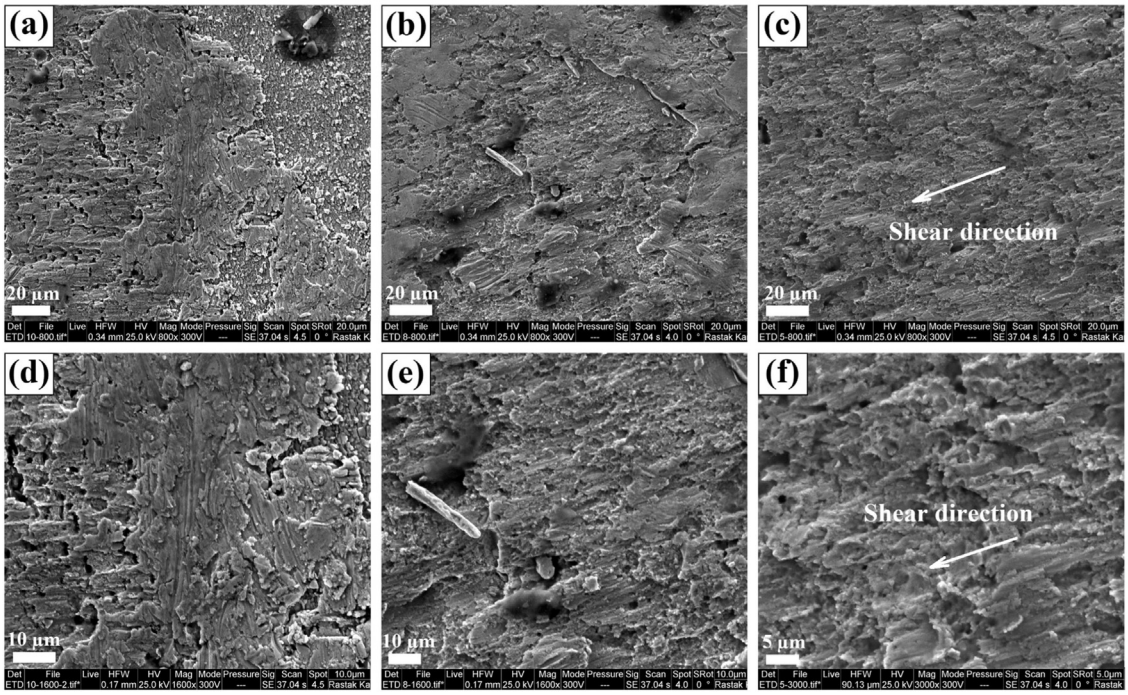

Fig. 20 – FE-SEM images from the fracture surfaces of failed nanocomposite soldered joints after aging treatment at a temperature of 150 °C for 100 h at two different magnifications; (a, d) 0.05 wt% GNPs, (b, e) 0.05 wt% Ni-GNPs, and (c, f) 0.1 wt% Ni-GNPs.

the highest value of ~27.3 MPa (an increasing ratio of ~23% as compared to the SAC solder alloy), where the flexibility continuously reduced down to ~12.4% (a reduction ratio of ~60%). These developments were found to be more severe in the presence of Ni-coating on the surface of nanoplatelets with the highest strength of ~28.3 MPa, despite more elongation loss.

- Isothermal aging was highlighted as a very effective treatment for simultaneous enhancement in shear strength and ductility of the soldered joints, especially in the presence of Ni-coating, up to the highest values of ~32.1 MPa and 19.9%, respectively. This post-processing action showed very operative by accelerating the diffusion of elements. As a result, dominant combined ductile-brittle fracture behavior was developed toward a more ductile failure.

Conflict of interest

The authors confirm that this work has no conflict of interest.

Acknowledgments

The partial financial support by the Austrian Federal Ministry for Digital and Economic Affairs and the National Foundation for Research, Technology, and Development are gratefully acknowledged.

Appendix A. Supplementary data

Supplementary data associated with this article can be found, in the online version, at doi:10.1016/j.jmrt.2020.06.026.

REFERENCES

[1] Humpston G, Jacobson DM. Principles of soldering and brazing. Materials Park, OH: ASM International; 1993.
[2] Zhang L, Tu KN. Structure and properties of lead-free solders bearing micro and nano particles. Mater Sci Eng R 2014;82(1):1–32.
[3] Kaushik RK, Batra U, Sharma JD. Aging induced structural and electrochemical corrosion behaviour of Sn-1.0Ag-0.5Cu and Sn-3.8Ag-0.7Cu solder alloys. J Alloys Compd 2018;745:446–54.
[4] Ma ZL, Shang H, Daszki AA, Belyakov SA, Gourlay CM. Mechanisms of beta-Sn nucleation and microstructure evolution in Sn–Ag–Cu solders containing titanium. J Alloys Compd 2019:1357–66.
[5] Bang J, Yu DY, Ko YH, Kim MS, Nishikawa H, Lee CW. Intermetallic compound formation and mechanical property of Sn-Cu-xCr/Cu lead-free solder joint. J Alloys Compd 2017;728:992–1001.
[6] El-Daly AA, Ibrahiem AA. The role of delayed elasticity and stress relaxation in Sn-Bi-Cu lead-free solders solidified under permanent magnet stirring. J Alloys Compd 2018;740:801–9.
[7] Javid NS, Sayyadi R, Khodabakhshi F. Lead-free Sn-based/MW-CNTs nanocomposite soldering: effects of reinforcing content, Ni-coating modification, and isothermal

ageing treatment. J. Mater Sci Mater Electron 2019;30(5):4737–52.
[8] Liu S, Zhang D, Xiong J, Chen C, Song T, Liu L, et al. Microstructure evolution and properties of rapidly solidified Au-20Sn eutectic solder prepared by single-roll technology. J Alloys Compd 2019:873–82.
[9] Tian F, Li CF, Zhou M, Liu ZQ. The interfacial reaction between In-48Sn solder and polycrystalline Cu substrate during solid state aging. J Alloys Compd 2018;740:500–9.
[10] Tian R, Hang C, Tian Y, Feng J. Brittle fracture induced by phase transformation of Ni-Cu-Sn intermetallic compounds in Sn-3Ag-0.5Cu/Ni solder joints under extreme temperature environment. J Alloys Compd 2019:463–71.
[11] Tian S, Li S, Zhou J, Xue F. Thermodynamic characteristics, microstructure and mechanical properties of Sn-0.7Cu-xIn lead-free solder alloy. J Alloys Compd 2018;742:835–43.
[12] El-Daly AA, Ibrahiem AA. Assessment of room-temperature short-term stress relaxation and strain relaxation with recovery in Sn-Bi lead-free solders solidified under rotating magnetic field. J Alloys Compd 2018;730:47–56.
[13] Rabiatul Adawiyah MA, Saliza Azlina O. Comparative study on the isothermal aging of bare Cu and ENImAg surface finish for Sn–Ag–Cu solder joints. J Alloys Compd 2018;740:958–66.
[14] El-Daly AA, Desoky WM, Elmosalami TA, El-Shaarawy MG, Abdraboh AM. Microstructural modifications and properties of SiC nanoparticles-reinforced Sn-3.0Ag-0.5Cu solder alloy. Mater Des 2015;65:1196–204.
[15] El-Daly AA, Fawzy A, Mansour SF, Younis MJ. Novel SiC nanoparticles-containing Sn-1.0Ag-0.5Cu solder with good drop impact performance. Mater Sci Eng A 2013;578:62–71.
[16] Wang X, Liu YC, Wei C, Gao HX, Jiang P, Yu LM. Strengthening mechanism of SiC-particulate reinforced Sn-3.7Ag-0.9Zn lead-free solder. J Alloys Compd 2009;480(2):662–5.
[17] Wu J, Xue S, Wang J, Wu M. Coupling effects of rare-earth Pr and Al_2O_3 nanoparticles on the microstructure and properties of Sn-0.3Ag-0.7Cu low-Ag solder. J Alloys Compd 2019;784:471–87.
[18] Chen G, Peng H, Silberschmidt VV, Chan YC, Liu C, Wu F. Performance of Sn-3.0Ag-0.5Cu composite solder with TiC reinforcement: physical properties, solderability and microstructural evolution under isothermal ageing. J Alloys Compd 2016;685:680–9.
[19] Gu Y, Zhao X, Li Y, Liu Y, Wang Y, Li Z. Effect of nano-Fe_2O_3 additions on wettability and interfacial intermetallic growth of low-Ag content Sn–Ag–Cu solders on Cu substrates. J Alloys Compd 2015;627:39–47.
[20] Hu X, Xu S, Yang Y, Chen Z, Chan YC. Effect of TiO_2 nanoparticle addition on electroless Ni-P under bump metallization for lead-free solder interconnection. Mater Sci Eng A 2014;600:67–75.
[21] Mohd Salleh MAA, McDonald SD, Nogita K. Effects of Ni and TiO_2 additions in as-reflowed and annealed Sn-0.7Cu solders on Cu substrates. J Mater Process Technol 2017;242:235–45.
[22] Eid EA, Fouda AN, Duraia ESM. Effect of adding 0.5wt% ZnO nanoparticles, temperature and strain rate on tensile properties of Sn-5.0wt% Sb-0.5wt% Cu (SSC505) lead free solder alloy. Mater Sci Eng A 2016;657:104–14.
[23] Sobhy M, El-Refai AM, Mousa MM, Saad G. Effect of ageing time on the tensile behavior of Sn-3.5 wt% Ag-0.5 wt% Cu (SAC355) solder alloy with and without adding ZnO nanoparticles. Mater Sci Eng A 2015;646:82–9.
[24] Mohd Salleh MAA, Bakri AMMA, Zan Hazizi MH, Somidin F, Mohd Alui NF, Ahmad ZA. Mechanical properties of Sn-0.7Cu/Si_3N_4 lead-free composite solder. Mater Sci Eng A 2012;556:633–7.
[25] Mohd Salleh MAA, Hazizi MHZ, Ahmad ZA, Hussin K, Ahmad KR. Wettability, electrical and mechanical properties of 99.3Sn-0.7Cu/Si_3N_4 novel lead-free nanocomposite solder. Adv Mater Res 2011:106–11.
[26] Sharma A, Das S, Das K. Electrochemical corrosion behavior of CeO_2 nanoparticle reinforced Sn-Ag based lead free nanocomposite solders in 3.5 wt.% NaCl bath. Surf Coat Technol 2015;261:235–43.
[27] Tsao LC. Evolution of nano-Ag_3Sn particle formation on Cu-Sn intermetallic compounds of Sn-3.5Ag-0.5Cu composite solder/Cu during soldering. J Alloys Compd 2011;509(5):2326–33.
[28] Sun R, Sui Y, Qi J, Wei F, He Y, Chen X, et al. Influence of SnO_2 nanoparticles addition on microstructure, thermal analysis, and interfacial IMC growth of Sn-1.0Ag-0.7Cu solder. J Electron Mater 2017;46(7):4197–205.
[29] Hu X, Chan YC. Reinforced solder joint performance by incorporation of ZrO_2 nanoparticles in electroless Ni-P composite layer. J Mater Res 2014;128(11):1–10.
[30] Sharma A, Baek BG, Jung JP. Influence of La_2O_3 nanoparticle additions on microstructure, wetting, and tensile characteristics of Sn–Ag–Cu alloy. Mater Des 2015;87:370–9.
[31] Bhattacharya S, Sharma A, Das S, Das K. Synthesis and properties of pulse electrodeposited lead-free tin-based Sn/$ZrSiO_4$ nanocomposite coatings. Metall Mater Trans A 2016;47(3):1292–312.
[32] Hu Z, Lu X. Chapter 8 – mechanical properties of carbon nanotubes and graphene A2 – Tanaka, K. In: Iijima S, editor. Carbon nanotubes and graphene. 2nd ed. Oxford: Elsevier; 2014. p. 165–200.
[33] Geim AK. Graphene: status and prospects. Science 2009;324(5934):1530–4.
[34] Geim AK, Novoselov KS. The rise of graphene. Nat Mater 2007;6(3):183–91.
[35] Lee C, Wei X, Kysar JW, Hone J. Measurement of the elastic properties and intrinsic strength of monolayer graphene. Science 2008;321(5887):385–8.
[36] Novoselov KS, Geim AK, Morozov SV, Jiang D, Katsnelson MI, Grigorieva IV, et al. Two-dimensional gas of massless Dirac fermions in graphene. Nature 2005;438(7065):197–200.
[37] Wei J, Zang Z, Zhang Y, Wang M, Du J, Tang X. Enhanced performance of light-controlled conductive switching in hybrid cuprous oxide/reduced graphene oxide (Cu_2O/rGO) nanocomposites. Opt Lett 2017;42(5):911–4.
[38] Liu X, Xu T, Li Y, Zang Z, Peng X, Wei H, et al. Enhanced X-ray photon response in solution-synthesized $CsPbBr_3$ nanoparticles wrapped by reduced graphene oxide. Sol Energy Mater Sol Cells 2018;187:249–54.
[39] Huang H, Zhang J, Jiang L, Zang Z. Preparation of cubic Cu_2O nanoparticles wrapped by reduced graphene oxide for the efficient removal of rhodamine B. J Alloys Compd 2017;718:112–5.
[40] Zang Z, Zeng X, Wang M, Hu W, Liu C, Tang X. Tunable photoluminescence of water-soluble AgInZnS–graphene oxide (GO) nanocomposites and their application in-vivo bioimaging. Sens Actuators B 2017;252:1179–86.
[41] Stankovich S, Dikin DA, Piner RD, Kohlhaas KA, Kleinhammes A, Jia Y, et al. Synthesis of graphene-based nanosheets via chemical reduction of exfoliated graphite oxide. Carbon 2007;45(7):1558–65.
[42] Bartolucci SF, Paras J, Rafiee MA, Rafiee J, Lee S, Kapoor D, et al. Graphene–aluminum nanocomposites. Mater Sci Eng A 2011;528(27):7933–7.
[43] Khodabakhshi F, Simchi A. The role of microstructural features on the electrical resistivity and mechanical properties of powder metallurgy Al-SiC-Al_2O_3 nanocomposites. Mater Des 2017;130:26–36.
[44] Nieto A, Bisht A, Lahiri D, Zhang C, Agarwal A. Graphene reinforced metal and ceramic matrix composites: a review. Int Mater Rev 2016:1–62.

[45] Chen G, Wu F, Liu C, Silberschmidt VV, Chan YC. Microstructures and properties of new Sn–Ag–Cu lead-free solder reinforced with Ni-coated graphene nanosheets. J Alloys Compd 2016;656:500–9.
[46] Jing HY, Guo HJ, Wang LX, Wei J, Xu LY, Han YD. Influence of Ag-modified graphene nanosheets addition into Sn–Ag–Cu solders on the formation and growth of intermetallic compound layers. J Alloys Compd 2017;702:669–78.
[47] Wang H, Zhang K, Zhang M. Fabrication and properties of Ni-modified graphene nanosheets reinforced Sn–Ag–Cu composite solder. J Alloys Compd 2019:761–72.
[48] Xu L, Wang L, Jing H, Liu X, Wei J, Han Y. Effects of graphene nanosheets on interfacial reaction of Sn–Ag–Cu solder joints. J Alloys Compd 2015;650:475–81.
[49] Xu LY, Zhang ST, Jing HY, Wang LX, Wei J, Kong XC, et al. Indentation size effect on Ag nanoparticle-modified graphene/Sn–Ag–Cu solders. J Electron Mater 2018;47(1):612–9.
[50] Xu LY, Zhang ZK, Jing HY, Wei J, Han YD. Effect of graphene nanosheets on the corrosion behavior of Sn–Ag–Cu solders. J Mater Sci Mater Electron 2015;26(8):5625–34.
[51] Khodabakhshi F, Sayyadi R, Javid NS. Lead free Sn–Ag–Cu solders reinforced by Ni-coated graphene nanosheets prepared by mechanical alloying: microstructural evolution and mechanical durability. Mater Sci Eng A 2017;702: 371–85.
[52] Xu L, Chen X, Jing H, Wang L, Wei J, Han Y. Design and performance of Ag nanoparticle-modified graphene/SnAgCu lead-free solders. Mater Sci Eng A 2016;667:87–96.
[53] Yoon JW, Lee YH, Kim DG, Kang HB, Suh SJ, Yang CW, et al. Intermetallic compound layer growth at the interface between Sn–Cu–Ni solder and Cu substrate. J Alloys Compd 2004;381(1–2):151–7.
[54] Yu DQ, Wu CML, Law CMT, Wang L, Lai JKL. Intermetallic compounds growth between Sn-3.5Ag lead-free solder and Cu substrate by dipping method. J Alloys Compd 2005;392(1–2):192–9.
[55] Mehrabi K, Khodabakhshi F, Zareh E, Shahbazkhan A, Simchi A. Effect of alumina nanoparticles on the microstructure and mechanical durability of meltspun lead-free solders based on tin alloys. J Alloys Compd 2016;688:143–55.
[56] Khodabakhshi F, Maleksaeedi S, Paydar MH, Saadat S. Influence of autogenous seeding on densification and microstructure in processing of γ-alumina nanopowders. Phase Transit 2011;84(1):1–14.
[57] Hu X, Chan YC, Zhang K, Yung KC. Effect of graphene doping on microstructural and mechanical properties of Sn-8Zn-3Bi solder joints together with electromigration analysis. J Alloys Compd 2013;580:162–71.
[58] Ma Y, Li X, Zhou W, Yang L, Wu P. Reinforcement of graphene nanosheets on the microstructure and properties of Sn-58Bi lead-free solder. Mater Des 2017;113:264–72.
[59] Sobhy M, El-Refai AM, Fawzy A. Effect of Graphene Oxide Nano-Sheets (GONSs) on thermal, microstructure and stress–strain characteristics of Sn-5 wt% Sb-1 wt% Ag solder alloy. J Mater Sci Mater Electron 2016;27(3):2349–59.
[60] Tsao LC. Suppressing effect of 0.5 wt.% nano-TiO_2 addition into Sn–3.5Ag–0.5Cu solder alloy on the intermetallic growth with Cu substrate during isothermal aging. J Alloys Compd 2011;509(33):8441–8.
[61] Khodabakhshi F, Arab SM, Švec P, Gerlich AP. Fabrication of a new Al-Mg/graphene nanocomposite by multi-pass friction-stir processing: dispersion, microstructure, stability, and strengthening. Mater Charact 2017;132:92–107.
[62] Khodabakhshi F, Nosko M, Gerlich AP. Effects of graphene nano-platelets (GNPs) on the microstructural characteristics and textural development of an Al-Mg alloy during friction-stir processing. Surf Coat Technol 2018;335:288–305.
[63] Aghajani Derazkola H, Khodabakhshi F. Intermetallic compounds (IMCs) formation during dissimilar friction-stir welding of AA5005 aluminum alloy to St-52 steel: numerical modeling and experimental study. Int J Adv Manuf Technol 2019;100(9–12):2401–22.
[64] Lee WB, Bang KS, Jung SB. Effects of intermetallic compound on the electrical and mechanical properties of friction welded Cu/Al bimetallic joints during annealing. J Alloys Compd 2005;390(1):212–9.
[65] Maleki M, Cugnoni J, Botsis J. Multi-scale modeling of elasto-plastic response of Sn–Ag–Cu lead-free solder alloys at different ageing conditions: effect of microstructure evolution, particle size effects and interfacial failure. Mater Sci Eng A 2016;661:132–44.